IEEE Access
Multidisciplinary | Rapid Review | Open Access Journal

Received April 13, 2020, accepted April 24, 2020, date of publication April 30, 2020, date of current version May 14, 2020.

Digital Object Identifier 10.1109/ACCESS.2020.2991396

Simple Finite-Control-Set Model Predictive Control of Grid-Forming Inverters With LCL Filters

HECTOR A. YOUNG [1], (Member, IEEE), VICTOR A. MARIN [2], CRISTIAN PESCE [1], (Member, IEEE), AND JOSE RODRIGUEZ [3], (Fellow, IEEE)

[1]Department of Electrical Engineering, Universidad de La Frontera, Temuco 4811230, Chile
[2]DAAB Ingenieria SpA, Osorno 5290000, Chile
[3]Faculty of Engineering, Universidad Andres Bello, Santiago 8370146, Chile

Corresponding author: Hector A. Young (hector.young@ufrontera.cl)

This work was supported in part by the Chilean National Commission for Science and Technology (CONICYT/ANID) under Grant FONDECYT 11160177, in part by the CONICYT/ANID, Advanced Center for Electrical and Electronic Engineering, under Grant FB-0008, and in part by the Universidad de La Frontera under Grant DI19-0013.

ABSTRACT Grid-forming inverters (GFI) play an important role as power interfaces for distributed generation units in islanded microgrids, where inductive-capacitive-inductive (LCL) output filters are commonly employed to mitigate the harmonics injected by voltage-source inverters. Due to advantages such as fast dynamic response and straightforward handling of constraints, Finite-control-set model predictive control (FCS-MPC) has become an attractive option for voltage control in GFI systems. However, conventional FCS-MPC algorithms with short prediction horizon have performance limitations in the tracking of ac references in systems with high-order dynamics, such as LCL-filtered GFIs. On the other hand, predictive algorithms with extended prediction horizons suffer from an increased computational burden. This paper proposes a new FCS-MPC algorithm to accurately control the capacitor voltage in an LCL-filtered GFI, using a discrete-time prediction model to dynamically compute the reference for a FCS-MPC inverter-side current controller. The main advantages of the proposed method are its simple implementation without requiring the tuning of weighting factors in its cost function; and its short prediction horizon, which maintains a reduced computational cost. Moreover, active resonance damping elements such as digital filters or ad hoc feedback loops to deal with the LCL filter resonance are not required. Simulation tests and experimental results in a laboratory-scale setup confirm the effectiveness of the proposed control algorithm, yielding lower distortion of output voltage waveforms and increased robustness to modeling errors compared with the conventional FCS-MPC approach.

INDEX TERMS DC-AC power converters, digital control, LCL filters, predictive control.

NOMENCLATURE

2L-VSI	Two-level voltage-source inverter
C_f	Filter capacitance
FCS-MPC	Finite-control-set model predictive control
g_{conv}	Cost function of the conventional FCS-MPC algorithm
g	Cost function of the proposed FCS-MPC algorithm
g_i, g_{lim}	Current tracking and current limiting components of cost function g
GFI	Grid-forming inverter
$\mathbf{i_i}$	Inverter current in the stationary $\alpha\beta$ frame
$i_{i\alpha}$, $i_{i\beta}$	α- and β-axis values of the inverter current
i_{ia}, i_{ib}, i_{ic}	Three-phase inverter currents
$\mathbf{i_i}^*$	Inverter current reference in the stationary $\alpha\beta$ frame
I_{max}	Preset inverter current limit
$\mathbf{i_o}$	Load current in the stationary $\alpha\beta$ frame
$i_{o\alpha}$, $i_{o\beta}$	α- and β-axis values of the load current
v_{oa}, v_{ob}, v_{oc}	Three-phase load voltages
k	Current time sampling instant
L_1, L_2	Inverter- and load-side inductances
LCL	Inductive-capacitive-inductive
N_p	Prediction horizon
PI	Proportional-integral

The associate editor coordinating the review of this manuscript and approving it for publication was Sze Sing Lee.

PWM	Pulse-width modulation
R_1, R_2	Parasitic resistances of the inverter- and load-side inductors
$\mathbf{S}_k$	Set of the inverter switching states S_a, S_b, S_c
THD	Total harmonic distortion
T_s	Sampling period for the FCS-MPC algorithms
$\mathbf{v_c}$	Capacitor voltage in the stationary $\alpha\beta$ frame
$v_{c\alpha}, v_{c\beta}$	α- and β-axis values of the capacitor voltage
v_{ca}, v_{cb}, v_{cc}	Three-phase capacitor voltages
$\mathbf{v_c}*$	Capacitor voltage reference in the stationary $\alpha\beta$ frame
$v^*_{c\alpha}, v^*_{c\beta}$	α- and β-axis values of the capacitor voltage reference
$\hat{v_{c\alpha}}, \hat{v_{c\beta}}$	Predicted values of the capacitor voltage in the stationary $\alpha\beta$ frame
V_{dc}	Dc-link voltage
$\mathbf{v_i}$	Inverter voltage in the stationary $\alpha\beta$ frame
$v_{i\alpha}, v_{i\beta}$	α- and β-axis values of the inverter voltage
v_{ia}, v_{ib}, v_{ic}	Three-phase inverter voltages
$\mathbf{v_o}$	Load voltage in the stationary $\alpha\beta$ frame
$v_{o\alpha}, v_{o\beta}$	α- and β-axis values of the load voltage
i_{oa}, i_{ob}, i_{oc}	Three-phase load currents
VR	Virtual resistance
ZOH	Zero-order hold

I. INTRODUCTION

Grid-forming inverters (GFI) are a key building block for islanded microgrids, acting as power interfaces to integrate distributed generation units to the electrical power system, and contributing with desirable features such as high-speed response and enhanced controllability [1]. GFIs operate as ac voltage sources, with amplitude and frequency set according to load requirements; therefore, high performance voltage control is mandatory to ensure a correct operation of the system [2].

The voltage control of a GFI is commonly implemented using a multiple-loop structure composed of linear controllers [3], where the bandwidth of the outer voltage loop needs to be several times smaller than that of the inner current loops to allow a decoupled control. This creates an intrinsic bandwidth limitation that affects the performance of higher control levels in applications such as microgrids with hierarchical structure [4]. Furthermore, in LCL inverter systems with pulse-width-modulation (PWM) voltage regulators, the stability depends strongly on the time delay introduced by the modulation process [5], making necessary the use of compensators and special tuning techniques for PI controllers, which increase the complexity of the solution [6]–[8].

Recently, finite-control-set model predictive control (FCS-MPC) has demonstrated to be a suitable alternative to PWM regulators in applications with LCL-filtered inverters [9], [10]. Among the advantages of FCS-MPC are its fast dynamic response, straightforward design of complex control objectives, as well as intuitive handling of nonlinearities and constraints [11]. Early works implemented simultaneous current tracking and filter resonance damping by integrating a frequency-dependent term in the cost function to penalize components that might excite LCL resonances [12]. The main drawback is the need of a band-pass digital filter tuned precisely at the resonant frequency, which makes the system vulnerable to parametric uncertainty, or complex resonance scenarios in systems with multiple paralleled inverters [13]. Adaptive filtering techniques may be employed to enhance the system robustness, but at the cost of higher complexity and computational cost [14].

FCS-MPC algorithms for voltage control of GFIs using one-step prediction horizons ($N_p = 1$) have the advantage of reduced computational burden [15], [16]. However, direct implementations of FCS-MPC with such a short prediction horizon lose accuracy in the tracking of sinusoidal references when higher order output filters are employed, leading to oscillations around the reference and increased distortion [17]. To overcome this issue, algorithms with extended prediction horizons have been employed. In [18], the same candidate output vector in a two-level voltage-source inverter (2L-VSI) is evaluated within two consecutive sampling periods, thus reducing the computational cost of sequential optimization steps. Longer prediction horizons have been combined with virtual resistance (VR) elements for resonance damping, resulting in low switching frequency and increased harmonic attenuation [19]. However, some VR schemes require the time derivative of either the capacitor or grid current, which can be difficult to obtain in practice due to high-frequency components.

A comprehensive study of FCS-MPC algorithms, considering different current feedbacks and multi-variable control, found that the most effective solution was grid-side current feedback control with long prediction horizon ($N_p = 6$), due to the third-order dynamics of the LCL filter and its inherent delay [20]. However, the use of longer prediction horizons is limited by the available computational power, considering that the number of calculations grows exponentially as the length of prediction horizon increases [18].

Alternative multi-variable FCS-MPC schemes that combine in a single cost function two or more of the system's state variables, namely inverter current, grid current and capacitor voltage, have been successfully implemented [20], [21]. In a different approach, a FCS-MPC voltage controller with a multi-objective cost function that simultaneously tracks the capacitor voltage reference and its derivative was proposed [17]. Nonetheless, the drawback of multi-objective approaches lies in the critical influence of weighting factors on the controller performance and the lack of standard tuning procedures for these parameters, which increases the design complexity [11]. Normally, the design of weighting factors is a time-consuming task that requires a large number of simulation runs and trial-and-error iterations. Automated methods for the design of these factors based on artificial intelligence have been recently proposed [22], but they still constitute an

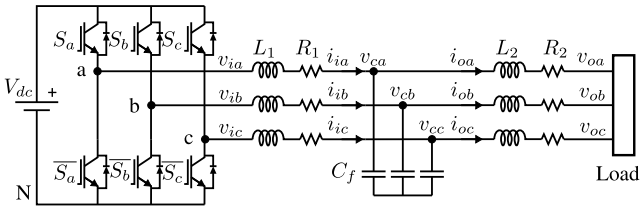

FIGURE 1. Three-phase two-level inverter with an LCL output filter.

additional component in the design process of the predictive controller.

This paper presents a new FCS-MPC strategy for capacitor voltage control of an LCL-filtered GFI, with reduced distortion using a short prediction horizon. A discrete mathematical model of the system is employed to dynamically compute an inverter-side current reference at a future sampling period, whose tracking results in the desired capacitor voltage behavior. Therefore, the original voltage control problem can be solved using a simple current-tracking FCS-MPC algorithm. The main features of the proposed controller are the following:

- The cost function of the FCS-MPC is designed only for current tracking, therefore the heuristic and time-consuming process of weighting factor tuning is avoided.
- No nested loop structures are required, thereby avoiding interactions between voltage and current control loops, and simplifying the controller design process.
- The proposed method does not require additional active damping elements such as frequency-sensitive components in the cost function [12] or filtered current feedback [23].
- The FCS-MPC is implemented with a short prediction horizon, keeping the computational burden low.

The remainder of this paper is organized as follows. In Section II a discrete model of the inverter and filter system is developed; in Section III the proposed control algorithm is explained in detail. Simulation and experimental results that confirm the effectiveness of the proposed controller and its robustness against modelling errors are presented in Sections IV and V, followed by the concluding comments in Section VI.

II. SYSTEM UNDER STUDY: VOLTAGE-SOURCE INVERTER WITH LCL FILTER

The schematic diagram of a 2L-VSI with an LCL output filter is presented in Fig. 1. The main passive elements of the system are the inverter- and load-side inductances, given by L_1 and L_2, respectively; and the filter capacitor C_f. Parasitic resistances of the inductors are represented by R_1, and R_2.

The dynamics of the system are modeled by the following set of equations:

$$\frac{d\mathbf{i_i}}{dt} = \frac{1}{L_1}\left(\mathbf{v_i} - R_1\mathbf{i_i} - \mathbf{v_c}\right) \tag{1}$$

$$\frac{d\mathbf{v_c}}{dt} = \frac{\mathbf{i_i} - \mathbf{i_o}}{C_f} \tag{2}$$

$$\frac{d\mathbf{i_o}}{dt} = \frac{1}{L_2}\left(\mathbf{v_c} - R_2\mathbf{i_o} - \mathbf{v_o}\right), \tag{3}$$

where $\mathbf{i_i}$ and $\mathbf{i_o}$ are the inverter and load currents, respectively; $\mathbf{v_i}$, $\mathbf{v_c}$ and $\mathbf{v_o}$ are the inverter, capacitor and load voltages, respectively. All the electrical variables in this model are represented as complex vectors in the stationary $\alpha\beta$ frame, and can be obtained from the corresponding three-phase voltages and currents using Clarke's transformation:

$$\mathbf{i_i} = i_{i\alpha} + ji_{i\beta} = \frac{2}{3}\left(i_{ia} + \mathbf{a}i_{ib} + \mathbf{a}^2\, i_{ic}\right) \tag{4}$$

$$\mathbf{i_o} = i_{o\alpha} + ji_{o\beta} = \frac{2}{3}\left(i_{oa} + \mathbf{a}i_{ob} + \mathbf{a}^2\, i_{oc}\right) \tag{5}$$

$$\mathbf{v_i} = v_{i\alpha} + jv_{i\beta} = \frac{2}{3}\left(v_{ia} + \mathbf{a}v_{ib} + \mathbf{a}^2\, v_{ic}\right) \tag{6}$$

$$\mathbf{v_c} = v_{c\alpha} + jv_{c\beta} = \frac{2}{3}\left(v_{ca} + \mathbf{a}v_{cb} + \mathbf{a}^2\, v_{cc}\right) \tag{7}$$

$$\mathbf{v_o} = v_{o\alpha} + jv_{o\beta} = \frac{2}{3}\left(v_{oa} + \mathbf{a}v_{ob} + \mathbf{a}^2 v_{oc}\right), \tag{8}$$

where $\mathbf{a} = e^{j2\pi/3}$ and v_{ia}, v_{ib}, v_{ic} are the inverter phase voltages with respect to the negative bus (N), which depend on the dc-link voltage V_{dc} and the switching states of each inverter leg S_a, S_b and S_c. The inverter voltage in vector notation can be expressed in terms of the switching states as:

$$\mathbf{v_i} = \frac{2}{3}V_{dc}\left(S_a + \mathbf{a}S_b + \mathbf{a}^2\, S_c\right) = V_{dc}\mathbf{S}, \tag{9}$$

where $\mathbf{S}$ is the $\alpha\beta$-frame representation of the switching states.

From the point of view of the predictive controller, with the objective of tracking a capacitor voltage reference, the mathematical model should be able to accurately predict the behavior of the controlled variable, i.e., $\mathbf{v_c}$. From (2) it is clear that the capacitor voltage dynamics is determined by the inverter current $\mathbf{i_i}$ and the load current $\mathbf{i_o}$. Therefore, for this control problem, if the load current can be measured, then it is not necessary to use (3) to predict its value, thus allowing to reduce the order of the prediction model.

Under this assumption, the system can be represented in a state-space form:

$$\dot{\mathbf{x}} = \mathbf{A}\mathbf{x}(t) + \mathbf{B}\mathbf{u}(t), \tag{10}$$

with state and input vectors defined as $\mathbf{x}(t) = [\mathbf{i_i}\ \mathbf{v_c}]^T$ and $\mathbf{u}(t) = [\mathbf{v_i}\ \mathbf{i_o}]^T$, respectively; matrices $\mathbf{A}$ and $\mathbf{B}$ are given by:

$$\mathbf{A} = \begin{bmatrix} -\frac{R_1}{L_1} & -\frac{1}{L_1} \\ \frac{1}{C_f} & 0 \end{bmatrix} \tag{11}$$

$$\mathbf{B} = \begin{bmatrix} \frac{1}{L_1} & 0 \\ 0 & -\frac{1}{C_f} \end{bmatrix}. \tag{12}$$

Predictive control algorithms require a discrete-time model of the system to calculate future values of the state variables

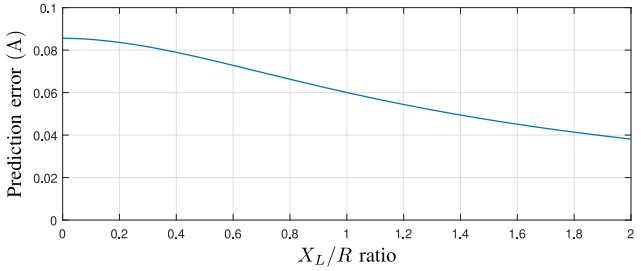

FIGURE 2. Absolute prediction error when assuming a constant load current within the prediction horizon.

starting from instantaneous measurements or estimations at the current sampling instant k. The discrete representation of the system (10) is given by:

$$\begin{bmatrix} \mathbf{i}_{\mathbf{i},k+1} \\ \mathbf{v}_{\mathbf{c},k+1} \end{bmatrix} = \mathbf{A_d} \begin{bmatrix} \mathbf{i}_{\mathbf{i},k} \\ \mathbf{v}_{\mathbf{c},k} \end{bmatrix} + \mathbf{B_d} \begin{bmatrix} \mathbf{v}_{\mathbf{i},k} \\ \mathbf{i}_{\mathbf{o},k} \end{bmatrix}. \tag{13}$$

Matrices $\mathbf{A_d}$ and $\mathbf{B_d}$ are computed through a zero-order-hold (ZOH) or exact discretization of the continuous system using a sampling period T_s [24]:

$$\mathbf{A_d} = e^{\mathbf{A}T_s} = \begin{bmatrix} a_{11} & a_{12} \\ a_{21} & a_{22}, \end{bmatrix} \tag{14}$$

$$\mathbf{B_d} = \int_0^{T_s} e^{\mathbf{A}\tau}\mathbf{B}d\tau = \begin{bmatrix} b_{11} & b_{12} \\ b_{21} & b_{22}, \end{bmatrix}, \tag{15}$$

where a_{ij} and b_{ij}, with $i, j \in \{1, 2\}$, are the numerical coefficients of matrices $\mathbf{A_d}$ and $\mathbf{B_d}$.

The main limitation of the reduced-order discrete-time model is that it is unable to predict future values of the load current $\mathbf{i_o}$. However, as explained later in Section III-B, the proposed controller requires predictions of this current up to sampling instant $k + 2$. To overcome this problem, in the control algorithm the load current is regarded as constant within the two future sampling periods after each measurement. To evaluate the validity of this assumption, simulation tests using a full-order discrete model and the parameters listed in Table 1 have been used to analyze the absolute prediction error in the load current, defined as $\left|\mathbf{i_o}_{k+2} - \mathbf{i_o}_k\right|$. The simulation results in Fig. 2 show the prediction error for a range of X_L/R ratios of the load side impedance. The absolute prediction error is below $[0.1]A$ and decreases for higher X_L/R ratios due to the higher inductance slowing down the dynamics of the load current. The average percent error in the whole range of load X_L/R ratios is $[1.89]\%$. From these results it is concluded that the assumption of constant load current in a limited time scale is valid, and the reduced order model can be used in the predictive algorithm.

III. PREDICTIVE VOLTAGE CONTROLLERS

The conventional FCS-MPC algorithm for capacitor voltage control in a GFI with LCL output filter, and the operating principles of the proposed FCS-MPC algorithm are explained in this section.

TABLE 1. System parameters.

Parameter	Value	Unit	Description
T_s	30	μs	Sampling period for FCS-MPC
C_f	33	μF	Filter capacitance
R_1, R_2	0.12	Ω	Inductor parasitic resistance
L_1	1.6	mH	Inverter-side filter inductance
L_2	1.6	mH	Load-side filter inductance
V_{dc}	200	V	DC-link voltage

A. CONVENTIONAL FCS-MPC

FCS-MPC algorithms for power converters use an exhaustive search optimization to generate the converter switching signals directly, without requiring a modulator [11]. The control objectives and constraints for the application are translated in a cost function, which is a measure of the divergence between the predicted response and the desired behavior of the system. This cost function is evaluated sequentially for each one of the feasible switching states of the power converter. Finally, an optimization procedure selects the switching state that produces the minimal value of the cost function. For voltage reference tracking in a three-phase VSI, the cost function of the conventional FCS-MPC in the $\alpha\beta$ frame is defined as [15]:

$$g_{\text{conv}} = \left(v^*_{c\alpha} - \hat{v_{c\alpha}}\right)^2 + \left(v^*_{c\beta} - \hat{v_{c\beta}}\right)^2, \tag{16}$$

where $v^*_{c\alpha}$, $v^*_{c\beta}$ and $\hat{v_{c\alpha}}$, $\hat{v_{c\beta}}$ are the reference and predicted values of the real and imaginary components of the capacitor voltage vector, respectively.

A challenge of controlling higher-order systems, such as the capacitor voltage of a GFI with LCL filter, using a short prediction horizon FCS-MPC is to accurately predict the effects of a future control action on the controlled variable within the prediction horizon. The ZOH discretization yields a model with relative degree equal to one, which theoretically allows controlling the output voltage using predictions up to the instant $k + 1$, i.e., with a prediction horizon $N_p = 1$ [25]. However, as can be deduced from the state-space model (10), the time-derivative of the capacitor voltage is not directly determined by the control input $\mathbf{v_i}$. This is reflected on the discrete-time model by very small values of the coefficient that connects the future state $\mathbf{v}_{\mathbf{c},k+1}$ with the input $\mathbf{v}_{\mathbf{i},k}$ in Eq. (13). Consequently, the capacitor voltage change is mainly determined by the inverter current and only slightly affected by the control input. Therefore, it takes a minimum of two sampling periods for the output to react to a control action, i.e., there is a minimal practical prediction horizon of $N_p = 2$. This issue has been previously pointed out as a limiting factor in applications of conventional FCS-MPC to inverter output voltage control with higher-order filters [17], [18], [20].

In applications of FCS-MPC the controller's performance is affected by a delay originated in the algorithm's computation time in digital processors. The duration of this delay differs greatly from that in PWM systems, which can be modeled as 1.5 times the PWM sampling period, and is about $[600]\mu s$

for typical applications [26], [27]. On the other hand, in FCS-MPC the delay amounts to a single sampling period, which in most applications using modern digital control platforms is shorter than [50]μs [28]. Therefore, computation delays that affect FCS-MPC are much smaller and easy to compensate than those of PWM controllers. An effective delay compensation technique consists on applying the optimal control action at the next sampling instant rather than immediately after the optimization process [29]. Adopting this compensation method implies that even in low-order systems where control with $N_p = 1$ is feasible, the predictions need to be evaluated up to the sampling instant $k + 2$.

B. PROPOSED CONTROLLER

As discussed in Section III-A, the minimal practical prediction horizon for capacitor voltage control in an LCL-filter is $N_p = 2$. However, taking into account the processing delay and the corresponding compensation method, this horizon needs to be extended to $N_p = 3$. Therefore, the control problem consists in selecting the inverter voltage vector to be applied to the system, so that the capacitor voltage can reach its reference at the future sampling instant $k + 3$.

From the discrete state-space model (13), and the numerical coefficients defined in equations (14) and (15), the predicted value of the capacitor voltage in the $\alpha\beta$ frame is given as:

$$\mathbf{v_c}_{,k+3} = a_{21}\mathbf{i_i}_{,k+2} + a_{22}\mathbf{v_c}_{,k+2} + b_{21}\mathbf{v_i}_{,k+2} + b_{22}\mathbf{i_o}_{,k+2}. \quad (17)$$

Accordingly, the inverter-side current that needs to be reached at the sampling instant $k + 2$ can be calculated from (17), substituting $\mathbf{v_c}_{,k+3}$ by its set-point value $\mathbf{v_c}^*_{,k+3}$:

$$\mathbf{i_i}^*_{,k+2} = \frac{\mathbf{v_c}^*_{,k+3} - a_{22}\mathbf{v_c}_{,k+2} - b_{21}\mathbf{v_i}_{,k+2} - b_{22}\mathbf{i_o}_{,k+2}}{a_{21}}. \quad (18)$$

Given that the voltage reference is designed at grid frequencies, it changes slowly in comparison with the sampling frequency of the FCS-MPC algorithm and the approximation $\mathbf{v_c}^*_{,k+3} \approx \mathbf{v_c}^*_{,k}$ can be employed. Moreover, the term $\mathbf{v_c}_{,k+2}$ can be readily predicted by iterating the discrete model (13).

Equation (18) requires the future value of the load current $\mathbf{i_o}_{,k+2}$, which can not be predicted using the reduced-order model (13). A simple approach is to consider that the load current is a slow-varying disturbance compared to the algorithm's high sampling frequency, as it is filtered by the load-side inductance L_2. Therefore, the load current is assumed to remain constant within the prediction horizon so it can be approximated by the instantaneous measured value, i.e., $\mathbf{i_o}_{,k+2} \approx \mathbf{i_o}_{,k}$. The same assumption is made with respect to the dc-link voltage measured at the sampling instant k, $V_{dc,k}$. The cost function for the proposed FCS-MPC algorithm is defined as:

$$g = g_i + g_{\text{lim}}, \quad (19)$$

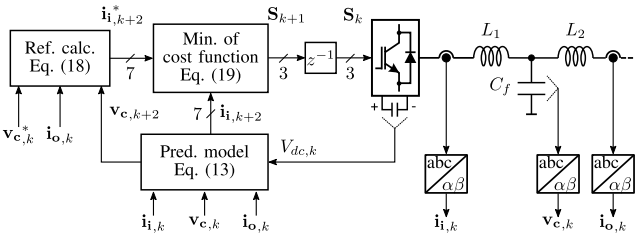

FIGURE 3. Block diagram of the proposed FCS-MPC algorithm.

where g_i has the purpose of tracking the current reference (18), and is defined in the $\alpha\beta$ frame as follows:

$$g_i = \left(i^*_{i\alpha,k+2} - i_{i\alpha,k+2}\right)^2 + \left(i^*_{i\beta,k+2} - i_{i\beta,k+2}\right)^2. \quad (20)$$

The second component of the cost function has the objective of penalizing control actions that would lead to unacceptably large currents, and is defined as:

$$g_{\text{lim}} = \begin{cases} ||\mathbf{i_i}_{,k+2}||, & \text{if } ||\mathbf{i_i}_{,k+2}|| \geq I_{\max} \\ 0, & \text{otherwise.} \end{cases} \quad (21)$$

The overcurrent term (21) activates only when the magnitude of the inverter current vector exceeds the preset limit $I_{\max}$. When active, g_{lim} takes the value of the current magnitude $||\mathbf{i_i}_{,k+2}||$, thereby favouring control actions that force the current down to normal values. It is important to note that the cost function (19) does not require the design of any weighting factors, despite having multiple components. This is because the current-limiting part should be zero in normal operating conditions.

The proposed FCS-MPC algorithm is represented by a block diagram in Fig. 3. The reference calculation block shown in the left uses the instantaneous capacitor voltage reference and load current measurements, together with the predicted capacitor voltage, to compute the inverter-side current reference for the FCS-MPC according to Eq. (18). The current tracking is performed by minimization of the cost function (19), using predictions given by the model established in (13).

A detailed description of the proposed FCS-MPC algorithm, executed in each control period, is given in Fig. 4 and consists in the following steps:

1) Measure voltages and currents in the system at the present sampling period (k): $\mathbf{i_i}_{,k}$, $\mathbf{v_c}_{,k}$, $\mathbf{i_o}_{,k}$ and $V_{dc,k}$.
2) Apply the optimal switching state $\mathbf{S}(j_{\text{op}})$, computed in the previous sampling interval. This memory operation is represented in Fig. 3 by a unitary delay at the input of the VSI's switching signals. The resulting voltage vector generated by the inverter, $\mathbf{v_i}_{,k}$, is given by (9).
3) Predict future values of the inverter current $\mathbf{i_i}_{,k+1}$ and capacitor voltage $\mathbf{v_c}_{,k+1}$ using (13). These predictions are computed using the inverter voltage vector produced in the previous step.
4) Evaluate the cost function (19) for each of the candidate control outputs, which belong to a set of seven

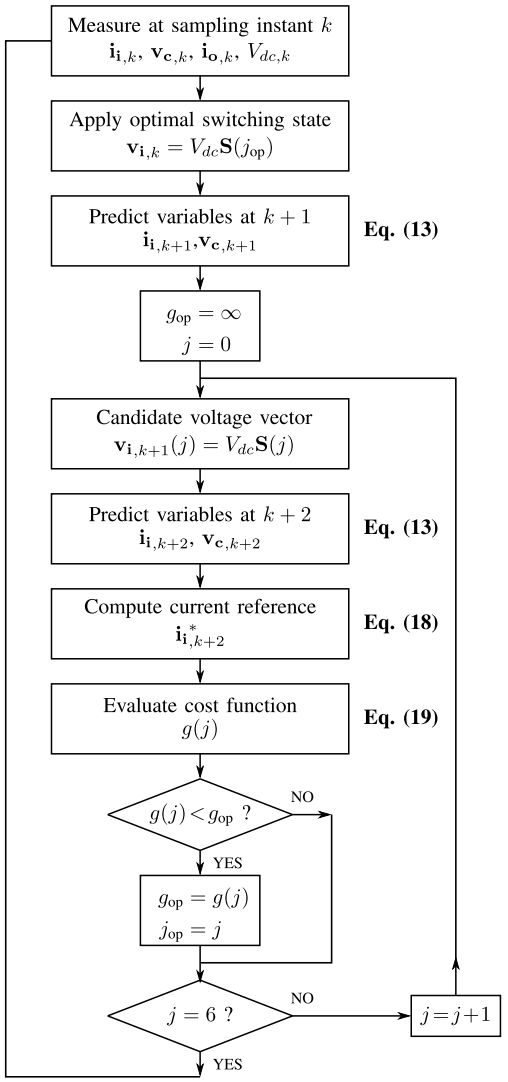

FIGURE 4. Flow diagram of the proposed FCS-MPC algorithm.

elements for a 2L-VSI, considering the redundancy of the zero voltage vector. The predicted values of $\mathbf{i}_{\mathbf{i},k+2}$ and $\mathbf{v}_{\mathbf{c},k+2}$ are computed using (13), whereas the inverter current reference to be tracked by the controller, $\mathbf{i}^*_{\mathbf{i},k+2}$, is obtained from (18).

5) Minimize over the set of cost function values to find the optimal control action. Store the optimal switching state to be applied on the next iteration of the algorithm.

IV. SIMULATION RESULTS

Simulation results using MATLAB/Simulink and PSim, interfaced through the SimCoupler module, are presented in order to validate the operation of the proposed FCS-MPC in a wide range of load-side impedance conditions. Fig. 5 shows steady-state waveforms of the capacitor voltage, obtained using both the conventional FCS-MPC and the proposed algorithm described in Sec. III-B.

In the case of Fig. 5(a) an X_L/R ratio of 0.02 is considered, which represents the operation with the system parameters

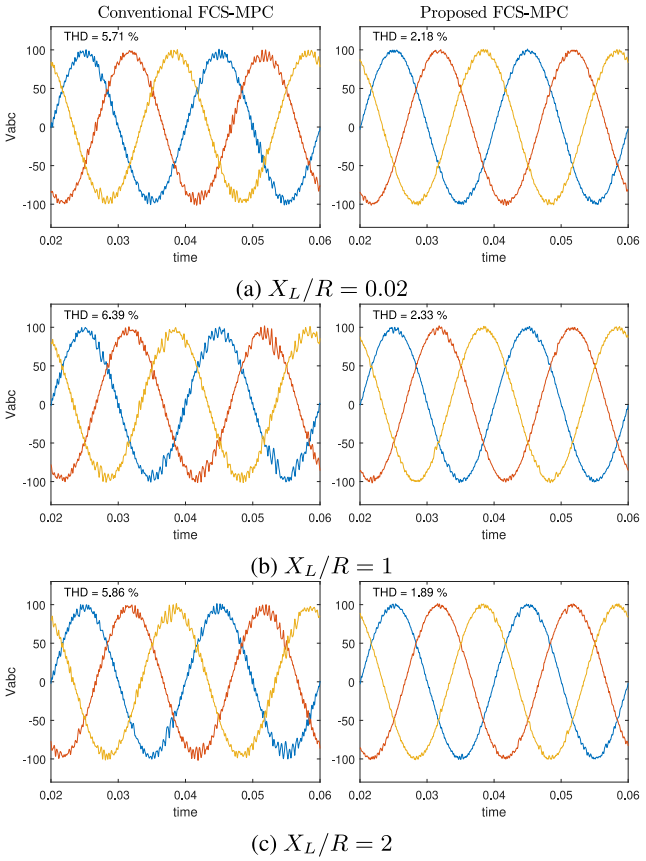

FIGURE 5. Simulation results: capacitor voltage control with the conventional (left column) and proposed (right column) FCS-MPC algorithms and diferent load-side impedance X_L/R ratios.

given in Table 1. The other cases consider a much larger inductance in the load side with X_L/R ratios of 1 and 2 for cases (b) and (c), respectively. It can be seen that both FCS-MPC algorithms are able to track the voltage references consistently, regardless the changes in the load impedance. However, the proposed FCS-MPC clearly presents lower distortion with reduced THD in all the tests. Moreover, the THD of the proposed FCS-MPC tends to reduce with increasing X_L/R ratios. This behavior is related to a reduction in the prediction error of the load current within the prediction horizon, as discussed in Sec. II and shown in Fig. 2.

V. EXPERIMENTAL RESULTS

Experimental tests were made to validate the proposed controller and to compare its performance against a conventional FCS-MPC algorithm. The power stage is composed by a Semikron Semiteach 2L-VSI with a three-phase LCL output filter and a $[4500]W$-rated resistive load. The control algorithms were implemented using a dSPACE DS1202 MicroLabBox compact prototyping unit, programmed in C language with Real-Time Library functions. Fig. 6 shows a photograph of the laboratory setup, and its main parameters are presented in Table 1. For inverter overcurrent protection, a current limit of $[10]A$ was set by means of the I_{max} parameter, defined in (21).

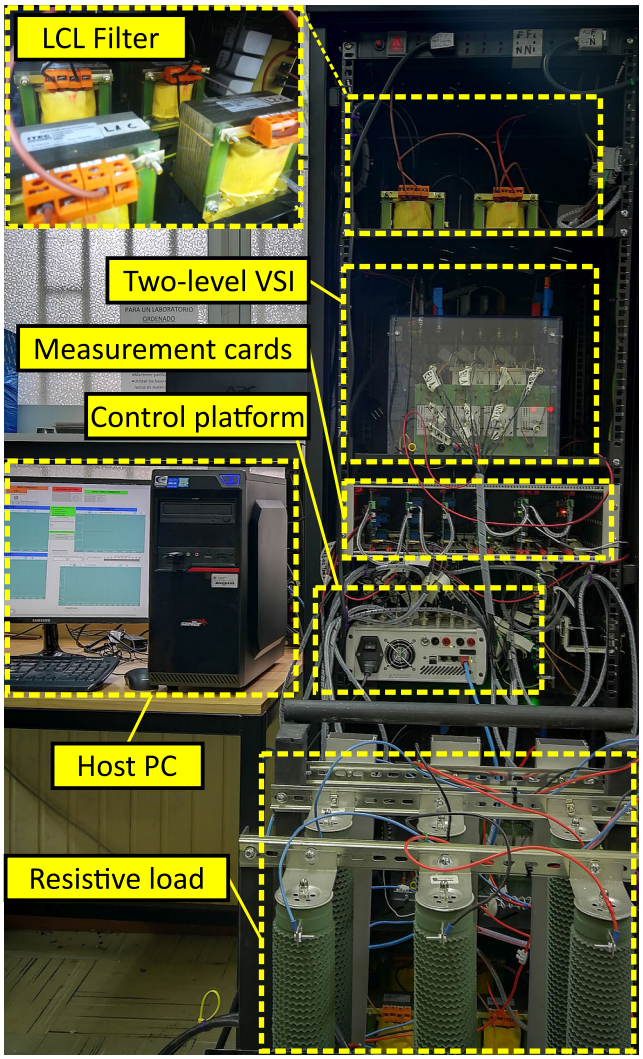

FIGURE 6. Photograph of the experimental setup.

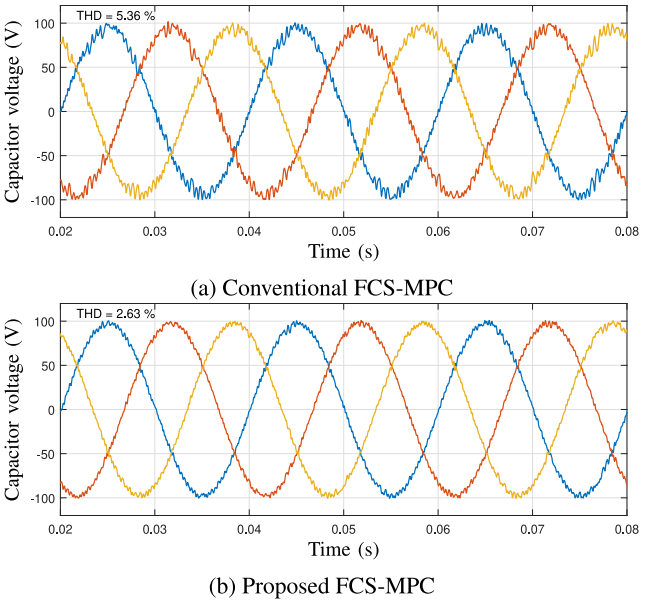

FIGURE 7. Experimental results: capacitor voltage control in steady state using (a) conventional and (b) the proposed FCS-MPC algorithm.

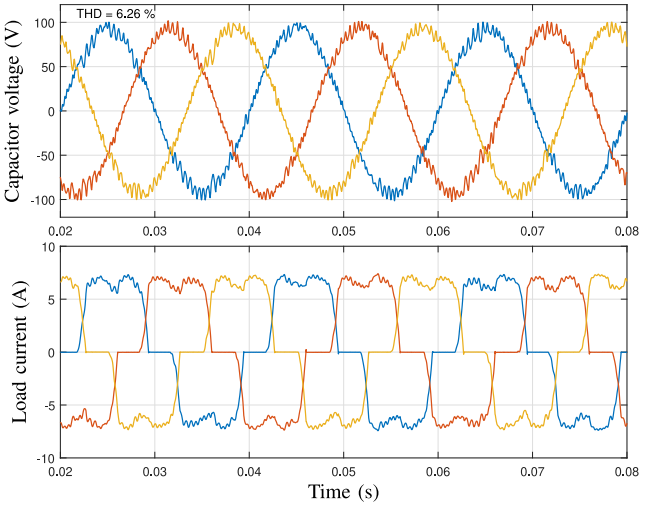

FIGURE 8. Experimental results of steady-state voltage control with conventional FCS-MPC and a non-linear load.

A. STEADY-STATE PERFORMANCE

The steady-state performance of both the conventional and the proposed FCS-MPC algorithms was evaluated while tracking a balanced three-phase sinusoidal voltage reference, with fixed amplitude and frequency of $[100]V$ and $[50]Hz$, respectively. A balanced three-phase $[22]\Omega$ resistor set was connected as a load. The results are presented in Fig. 7, comparing the three-phase voltage waveforms obtained with the two controllers. The proposed FCS-MPC achieved a 50.9% lower total harmonic distortion (THD) than that of the conventional controller.

B. NON-LINEAR LOAD

A Semikron SKD 51/14 full-bridge diode rectifier with a capacitive output filter of $[1100]\mu F$ and a resistive load of $[22]\Omega$ was employed to test the performance of the predictive voltage controllers operating with a non-linear load. The results are presented in Figs. 8 and 9 for the conventional and the proposed FCS-MPC algorithms, respectively. In this case the proposed FCS-MPC also presented a lower voltage THD with $[3.02]\%$ versus the $[6.26]\%$ obtained with the conventional algorithm, which implies a reduction of $[51.76]\%$ in the voltage distortion.

A summary of the steady-state performance of both the conventional and the proposed FCS-MPC algorithms, with linear and non-linear loads, is presented in Table 2.

C. PERFORMANCE UNDER LOAD AND REFERENCE DISTURBANCES

To assess the transient performance and disturbance rejection capability of the proposed predictive algorithm, two tests were carried out. The first one considered a load step change by connecting an additional $[22]\Omega$ three-phase resistor bank

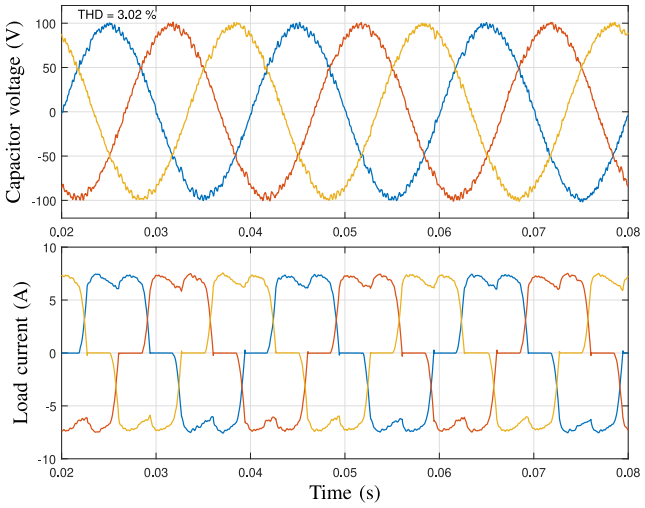

FIGURE 9. Experimental results of steady-state voltage control with the proposed FCS-MPC and a non-linear load.

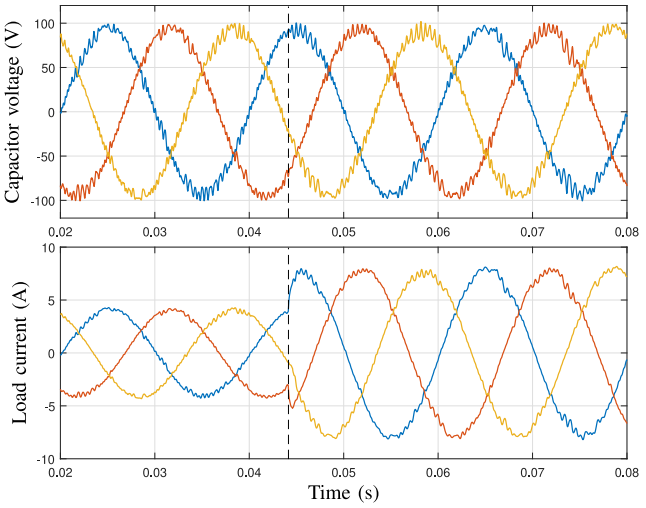

FIGURE 10. Experimental test of the transient response to a +100% load step change with conventional FCS-MPC.

TABLE 2. Performance comparison of the FCS-MPC algorithms.

Steady-state			
Criterion	Conventional	Proposed	Comparison
Linear load Voltage THD	5.36 %	2.63 %	−50.93 %
Non-linear load Voltage THD	6.26 %	3.02 %	−51.76 %
Transient response after a reference step change			
Criterion	Conventional	Proposed	Comparison
Overshoot	88.64 %	61.58 %	−30.53 %
Settling time (10 %)	1.38 ms	0.54 ms	−60.87 %

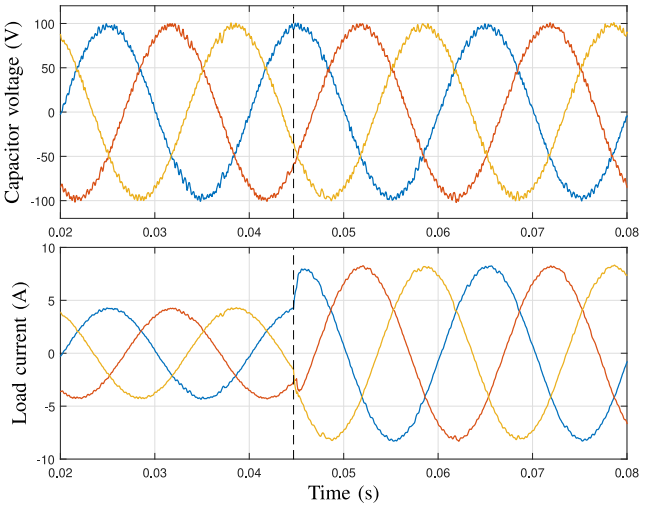

FIGURE 11. Experimental test of the transient response to a +100% load step change with the proposed FCS-MPC.

in parallel with the nominal load. The second test consisted in a reference amplitude step change from the nominal $[100]V$ to $[50]V$.

The results of the load step change for both the conventional and the proposed FCS-MPC algorithms are presented in Figs. 10 and 11, respectively, where the instant of the load step is marked with a dashed line. In Fig. 10 it is clear that after the load impact the conventional FCS-MPC exhibits increased voltage and load current oscillations. On the other hand, the proposed FCS-MPC maintained its steady-state performance both in voltage and currents, showing a superior load disturbance rejection performance.

The responses of both the predictive controllers to a reference step change from $[100]V$ to $[50]V$ in amplitude are detailed in Fig. 12, with the resulting voltage waveforms presented in the $\alpha\beta$ frame. It can be observed that the conventional FCS-MPC exhibits a more oscillatory response than the proposed algorithm. Table 2 summarizes the transient performance of the predictive controllers in terms of percentage overshoot and settling time to a 10% band around the reference. In terms of these indices, the proposed FCS-MPC shows a superior performance with a $[30.53]\%$ smaller overshoot and a $[60.87]\%$ smaller settling time compared with the conventional approach.

D. PERFORMANCE UNDER MODELING ERRORS

The robustness of the proposed FCS-MPC against parametric modeling errors has been experimentally evaluated by using mismatched values of the main parameters in the prediction model. As can be seen from (11) and (12), only the inverter-side inductance L_1, its parasitic resistance R_1 and the filter capacitance C_f are relevant in the dynamic model of the system. The load-side filter components and load parameters are not part of the prediction model, under the assumption that the disturbance current $\mathbf{i_o}$ can be measured or estimated.

The steady-state voltage waveforms obtained with the proposed FCS-MPC under various parametric modeling errors are presented in Fig. 13. In each case the parameter value used to compute the discrete model was either increased or decreased by a $[50]\%$ with respect to the physical values of the filter elements given in Table 1. These results show that even under severe errors in the parameter values used

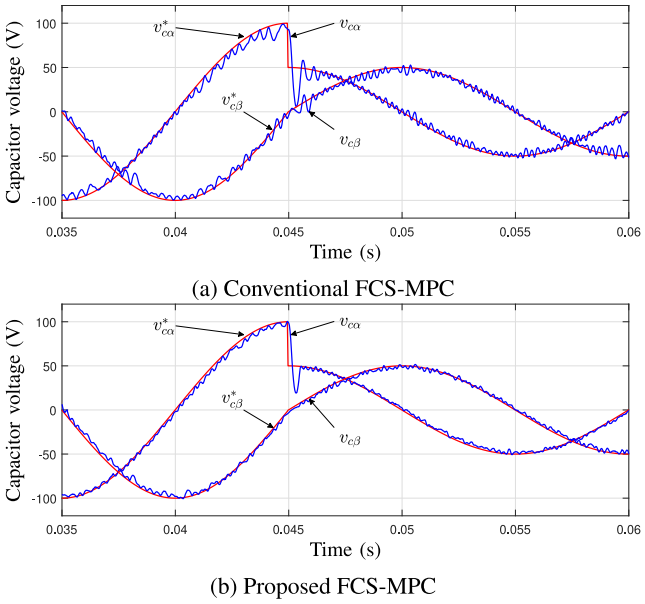

(a) Conventional FCS-MPC

(b) Proposed FCS-MPC

FIGURE 12. Experimental comparison of the transient response to a −50% reference step-change with (a) conventional and (b) the proposed FCS-MPC algorithms. Results shown in the $\alpha\beta$ frame.

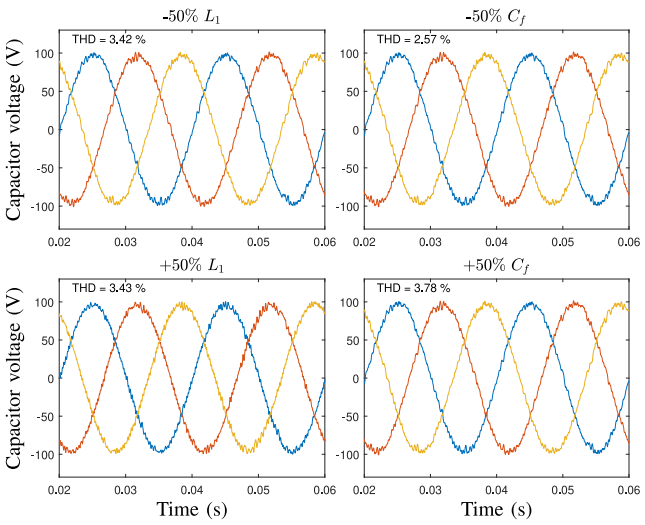

FIGURE 13. Experimental steady-state voltage waveforms with the proposed FCS-MPC under modeling errors in the filter parameters. Inverter-side inductance L_1 −[50]% (top left), +[50]% (bottom left); filter capacitance C_f −[50]% (top right), +[50]% (bottom right).

in the prediction model, the proposed FCS-MPC remains stable and with distortion limits close to its performance in the nominal case.

The variation of voltage THD is presented in Fig. 14 for several degrees of modeling error in the inverter-side inductance (L_1), filter capacitance (C_f) and inverter-side inductor parasitic resistance (R_1). The voltage THD obtained with the proposed FCS-MPC considering modeling inaccuracy in R_1 is presented in Fig. 14(a). Changes of ±[100]% and ±[50]% were applied in experimental tests, showing negligible effects on the voltage distortion. For L_1, parametric errors ranging from −[50]% to +[50]% with increments of [10]% were

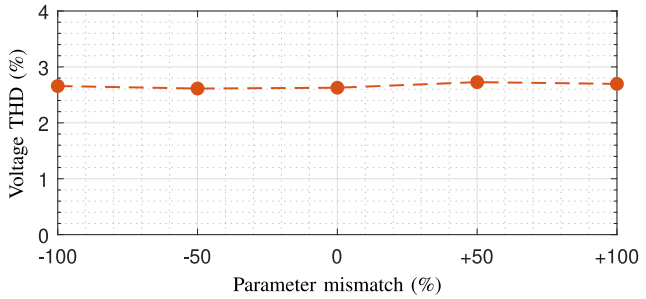

(a) Inverter-side inductor parasitic resistance (R_1).

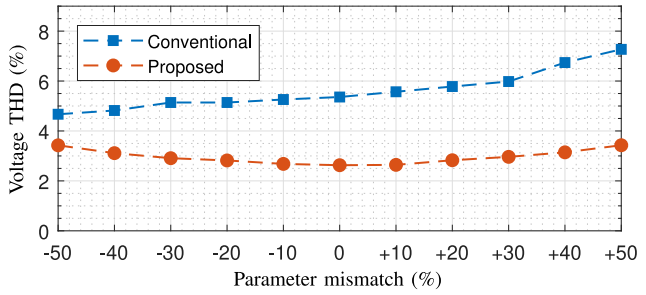

(b) Inverter-side inductance (L_1).

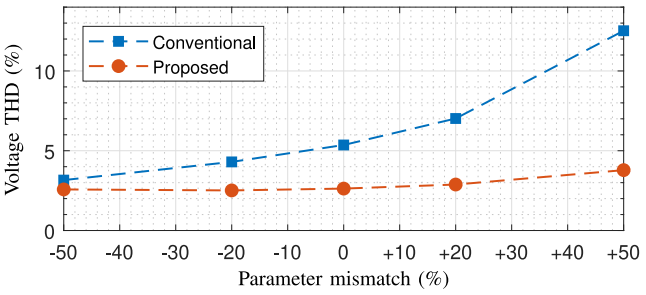

(c) Filter capacitance (C_f).

FIGURE 14. Voltage THD of experimental waveforms under modeling errors in the filter parameters: (a) inverter-side inductor parasitic resistance R_1 (proposed FCS-MPC), (b) inverter-side inductance L_1 and (c) filter capacitance C_f.

considered. In Fig. 14b), the proposed controller showed a slight rise in the voltage THD for increasing modeling errors of the filter inductance, whereas the minimal THD is achieved when L_1 is set to its nominal value. In this case, the variation of voltage THD is symmetrical, indicating that under- or over-estimating the value of L_1 has roughly the same effect on the voltage quality. On the other hand, conventional FCS-MPC presents higher voltage THD in all the cases, with an evident increase in tests where the modeled inductance is higher than the real parameter value.

Fig. 14(c) shows the changes of voltage THD for ±[50]% and ±[20]% modeling errors in C_f. In this case the THD changes asymmetrically, indicating that the use of C_f values larger than the real capacitance has a more detrimental effect than underestimating this parameter value. In fact, the minimal voltage THD was observed with a C_f value [20]% lower than the real capacitance. Comparing the performance of both predictive algorithms, the proposed controller keeps a voltage THD below [4]% in all the tested conditions, whereas conventional FCS-MPC shows a distortion level

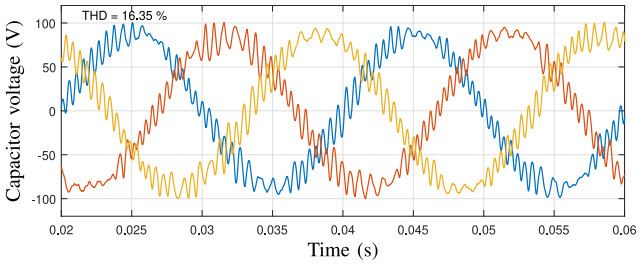

(a) Conventional FCS-MPC.

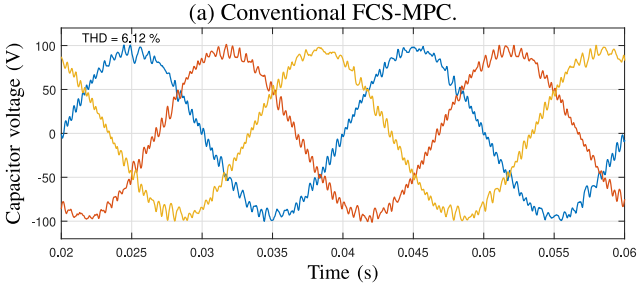

(b) Proposed FCS-MPC.

FIGURE 15. Experimental results: steady-state voltage with simultaneous +50% parameter mismatch of inverter-side inductance and capacitance with (a) conventional and (b) the proposed FCS-MPC.

higher than [10]% in the case where filter capacitance is overestimated by [50]%.

Fig. 15 shows the steady-state voltage waveforms obtained with the FCS-MPC algorithms considering simultaneous modeling errors in L_1 and C_f. The degree of mismatch that led to the highest THD was selected, that is, + [50]% for each parameter. Even though the THD level with the proposed FCS-MPC is significantly higher than in the nominal case of Fig. 7(b), its performance is clearly superior than that of the conventional algorithm in terms of robustness to modeling errors.

VI. CONCLUSION

In this paper, a simple and effective FCS-MPC algorithm for the capacitor voltage control in a 2L-VSI with output LCL filter has been developed. The proposed controller does not require weighting factors in the cost function, which greatly simplifies the design process. Moreover, it is implemented with a short prediction horizon, thereby keeping the computational cost low.

Simulations and experimental tests using a laboratory scale setup were carried out to show the feasibility and effectiveness of the proposed method. Compared to a conventional FCS-MPC algorithm, the proposed controller achieved a superior reference tracking performance with reduced harmonic distortion. Furthermore, the proposed controller demonstrated a higher robustness to variations of the filter parameters than the conventional FCS-MPC.

REFERENCES

[1] B. Kroposki, C. Pink, R. DeBlasio, H. Thomas, M. Simães, and P. K. Sen, "Benefits of power electronic interfaces for distributed energy systems," *IEEE Trans. Energy Convers.*, vol. 25, no. 3, pp. 901–908, Sep. 2010.

[2] J. M. Guerrero, M. Chandorkar, T.-L. Lee, and P. C. Loh, "Advanced control architectures for intelligent microgrids—Part I: Decentralized and hierarchical control," *IEEE Trans. Ind. Electron.*, vol. 60, no. 4, pp. 1254–1262, Apr. 2013.

[3] J. Rocabert, A. Luna, F. Blaabjerg, and P. Rodríguez, "Control of power converters in AC microgrids," *IEEE Trans. Power Electron.*, vol. 27, no. 11, pp. 4734–4749, Nov. 2012.

[4] J. M. Guerrero, J. C. Vasquez, J. Matas, L. G. de Vicuna, and M. Castilla, "Hierarchical control of droop-controlled AC and DC microgrids—A general approach toward standardization," *IEEE Trans. Ind. Electron.*, vol. 58, no. 1, pp. 158–172, Jan. 2011.

[5] J. Wang, J. D. Yan, L. Jiang, and J. Zou, "Delay-dependent stability of single-loop controlled grid-connected inverters with LCL filters," *IEEE Trans. Power Electron.*, vol. 31, no. 1, pp. 743–757, Jan. 2016.

[6] Z. Xin, X. Wang, P. C. Loh, and F. Blaabjerg, "Grid-current-feedback control for LCL-filtered grid converters with enhanced stability," *IEEE Trans. Power Electron.*, vol. 32, no. 4, pp. 3216–3228, Apr. 2017.

[7] C. Chen, J. Xiong, Z. Wan, J. Lei, and K. Zhang, "A time delay compensation method based on area equivalence for active damping of an LCL-type converter," *IEEE Trans. Power Electron.*, vol. 32, no. 1, pp. 762–772, Jan. 2017.

[8] L. Antonio de Souza Ribeiro, F. D. Freijedo, F. de Bosio, M. S. Lima, J. M. Guerrero, and M. Pastorelli, "Full discrete modeling, controller design, and sensitivity analysis for high-performance grid-forming converters in islanded microgrids," *IEEE Trans. Ind. Appl.*, vol. 54, no. 6, pp. 6267–6278, Nov. 2018. [Online]. Available: https://ieeexplore.ieee.org/document/8386696/

[9] E. Zangeneh Bighash, S. M. Sadeghzadeh, E. Ebrahimzadeh, and F. Blaabjerg, "High quality model predictive control for single phase grid-connected photovoltaic inverters," *Electric Power Syst. Res.*, vol. 158, pp. 115–125, May 2018.

[10] E. Zangeneh Bighash, S. M. Sadeghzadeh, E. Ebrahimzadeh, and F. Blaabjerg, "Robust MPC-based current controller against grid impedance variations for single-phase grid-connected inverters," *ISA Trans.*, vol. 84, pp. 154–163, Jan. 2019.

[11] S. Vazquez, J. Rodriguez, M. Rivera, L. G. Franquelo, and M. Norambuena, "Model predictive control for power converters and drives: Advances and trends," *IEEE Trans. Ind. Electron.*, vol. 64, no. 2, pp. 935–947, Feb. 2017.

[12] H. Miranda, R. Teodorescu, P. Rodriguez, and L. Helle, "Model predictive current control for high-power grid-connected converters with output LCL filter," in *Proc. 35th Annu. Conf. IEEE Ind. Electron.*, Nov. 2009, pp. 633–638.

[13] J. He, Y. W. Li, D. Bosnjak, and B. Harris, "Investigation and active damping of multiple resonances in a parallel-inverter-based microgrid," *IEEE Trans. Power Electron.*, vol. 28, no. 1, pp. 234–246, Jan. 2013.

[14] S. C. Ferreira, R. B. Gonzatti, R. R. Pereira, C. H. da Silva, L. E. B. da Silva, and G. Lambert-Torres, "Finite control set model predictive control for dynamic reactive power compensation with hybrid active power filters," *IEEE Trans. Ind. Electron.*, vol. 65, no. 3, pp. 2608–2617, Mar. 2018.

[15] P. Cortes, G. Ortiz, J. I. Yuz, J. Rodriguez, S. Vazquez, and L. G. Franquelo, "Model predictive control of an inverter with output *LC* filter for UPS applications," *IEEE Trans. Ind. Electron.*, vol. 56, no. 6, pp. 1875–1883, Jun. 2009.

[16] V. Yaramasu, M. Rivera, M. Narimani, B. Wu, and J. Rodriguez, "Model predictive approach for a simple and effective load voltage control of four-leg inverter with an output *LC* filter," *IEEE Trans. Ind. Electron.*, vol. 61, no. 10, pp. 5259–5270, Oct. 2014.

[17] T. Dragicevic, "Model predictive control of power converters for robust and fast operation of AC microgrids," *IEEE Trans. Power Electron.*, vol. 33, no. 7, pp. 6304–6317, Jul. 2018.

[18] P. Cortes, J. Rodriguez, S. Vazquez, and L. G. Franquelo, "Predictive control of a three-phase UPS inverter using two steps prediction horizon," in *Proc. IEEE Int. Conf. Ind. Technol.*, Mar. 2010, pp. 1283–1288.

[19] J. Scoltock, T. Geyer, and U. K. Madawala, "A model predictive direct current control strategy with predictive references for MV grid-connected converters with *LCL*-filters," *IEEE Trans. Power Electron.*, vol. 30, no. 10, pp. 5926–5937, Oct. 2015.

[20] N. Panten, N. Hoffmann, and F. W. Fuchs, "Finite control set model predictive current control for grid-connected voltage-source converters with LCL filters: A study based on different state feedbacks," *IEEE Trans. Power Electron.*, vol. 31, no. 7, pp. 5189–5200, Jul. 2016.

[21] P. Falkowski and A. Sikorski, "Finite control set model predictive control for grid-connected AC–DC converters with LCL filter," *IEEE Trans. Ind. Electron.*, vol. 65, no. 4, pp. 2844–2852, Apr. 2018.
[22] T. Dragicevic and M. Novak, "Weighting factor design in model predictive control of power electronic converters: An artificial neural network approach," *IEEE Trans. Ind. Electron.*, vol. 66, no. 11, pp. 8870–8880, Nov. 2019.
[23] E. Rodriguez-Diaz, F. D. Freijedo, J. C. Vasquez, and J. M. Guerrero, "Analysis and comparison of notch filter and capacitor voltage feedforward active damping techniques for LCL grid-connected converters," *IEEE Trans. Power Electron.*, vol. 34, no. 4, pp. 3958–3972, Apr. 2019.
[24] G. C. Goodwin, S. F. Graebe, and M. E. Salgado, *Control System Design*, 1st ed. Upper Saddle River, NJ, USA: Prentice-Hall, 2000.
[25] C. A. Silva and J. I. Yuz, "On sampled-data models for model predictive control," in *Proc. 36th Annu. Conf. IEEE Ind. Electron. Soc. (IECON)*, Nov. 2010, pp. 2966–2971.
[26] B.-H. Bae and S.-K. Sul, "A compensation method for time delay of full-digital synchronous frame current regulator of PWM AC drives," *IEEE Trans. Ind. Appl.*, vol. 39, no. 3, pp. 802–810, May 2003.
[27] C. S. Lim, S. S. Lee, Y. C. Cassandra Wong, I. U. Nutkani, and H. H. Goh, "Comparison of current control strategies based on FCS-MPC and D-PI-PWM control for actively damped VSCs with LCL-filters," *IEEE Access*, vol. 7, pp. 112410–112423, 2019. [Online]. Available: https://ieeexplore.ieee.org/document/8793070/
[28] S. Vazquez, J. I. Leon, L. G. Franquelo, J. Rodriguez, H. A. Young, A. Marquez, and P. Zanchetta, "Model predictive control: A review of its applications in power electronics," *IEEE Ind. Electron. Mag.*, vol. 8, no. 1, pp. 16–31, Mar. 2014.
[29] P. Cortes, J. Rodriguez, C. Silva, and A. Flores, "Delay compensation in model predictive current control of a three-phase inverter," *IEEE Trans. Ind. Electron.*, vol. 59, no. 2, pp. 1323–1325, Feb. 2012.

HECTOR A. YOUNG (Member, IEEE) was born in Valparaiso, Chile, in 1984. He received the B.Eng. and M.Sc. degrees in electronics engineering from the Universidad de la Frontera, Temuco, Chile, in 2009, and the Ph.D. degree in power electronics from Universidad Tecnica Federico Santa Maria, Valparaiso, in 2014.

Since 2014, he has been an Assistant Professor with the Electrical Engineering Department, Universidad de La Frontera. His research interests include modeling and control of power converters and electrical drives, renewable energy systems, and microgrids.

VICTOR A. MARIN was born in Montevideo, Uruguay, in 1986. He received the B.Eng. degree in electrical engineering from the Universidad de La Frontera, Temuco, Chile, in 2018.

From 2018 to 2019, he was a Research Assistant with the Electrical Engineering Department, Universidad de La Frontera. He is currently with DAAB Ingenieria SpA, Osorno, Chile, as a Project Engineer. His research interests include industrial automation, control of power converters, and renewable energy technologies.

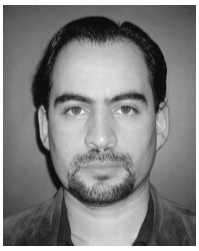

CRISTIAN PESCE (Member, IEEE) was born in Rancagua, Chile, in 1975. He received the degree in electronic engineering from the Pontificia Universidad Catolica de Valparaiso, Valparaiso, Chile, in 2003, the M.Sc. degree from the Universidad de La Frontera, Temuco, Chile, in 2010, and the D.Sc. degree from the Universidad de Concepcion, Concepcion, Chile, in 2017. He is currently a Lecturer with the Electrical Engineering Department, Universidad de La Frontera. His research interests include design and control of power converters applied to power systems, and direct current, and AC drives.

JOSE RODRIGUEZ (Fellow, IEEE) received the bachelor's degree in electrical engineering from Universidad Tecnica Federico Santa Maria, Valparaiso, Chile, in 1977, and the Dr.-Ing. degree in electrical engineering from the University of Erlangen, Erlangen, Germany, in 1985. He has been with the Department of Electronics Engineering, Universidad Tecnica Federico Santa Maria, since 1977, where he was a Full Professor and the President. Since 2015, he has been the President and since 2019, he has been a Full Professor with Universidad Andres Bello, Santiago, Chile. He has coauthored two books, several book chapters, and more than 400 journal and conference papers. His main research interests include multilevel inverters, new converter topologies, control of power converters, and adjustable-speed drives. He is a member of the Chilean Academy of Engineering. He has received a number of best paper awards from journals of the IEEE. In 2014, he received the National Award of Applied Sciences and Technology from the government of Chile. In 2015, he received the Eugene Mittelmann Award from the Industrial Electronics Society of the IEEE. From 2014 to 2019, he has been included in the list of Highly Cited Researchers published by Web of Science.